

## Fermi-level effects in *a*-Si:H photoconductivity

Toshiaki Kagawa, Nobuo Matsumoto, and Kenji Kumabe

*Musashino Electrical Communication Laboratory, Nippon Telegraph and Telephone Public Corporation, Musashino-shi, Tokyo 180, Japan*

(Received 3 September 1982; revised manuscript received 1 July 1983)

Fermi-level—position effects on photoconductivity in *a*-Si:H were studied using metal-oxide-semiconductor field-effect transistor devices. When the Fermi level shifts toward the conduction band as a result of field effect, the photoconductive current increases monotonically without saturation and the exponent of its illumination intensity dependence is gradually reduced from 0.9 to 0.4. These features can be explained if photoexcited electrons are distributed among extended states and localized states and if the nonradiative-recombination rate through recombination centers is controlled by the free-hole—capture rate of the recombination centers.

### I. INTRODUCTION

Recombination mechanisms for photoexcited carriers in *a*-Si:H have been investigated by using several methods, including photoluminescence,<sup>1,2</sup> transient photoconductivity,<sup>3,4</sup> photoinduced absorption,<sup>5</sup> and photoconductive sensitivity.<sup>6,7</sup> Photoluminescence is a highly effective method for investigating radiative recombination at low temperature, but it cannot be used for nonradiative recombination at room temperature. The transient photoconductivity method is very complex, because it is influenced by time-dependent mobility as well as by recombination. Therefore, it is difficult to obtain information about recombination. On the other hand, the photoconductive sensitivity and the illumination power dependence of the photocurrent directly reflect the recombination mechanism.

Anderson and Spear<sup>6</sup> reported that the exponent  $\gamma$  of illumination power dependence changed from 1.0 to 0.5 when the Fermi level was shifted by phosphorus doping. They attributed this phenomenon to a transition from a monomolecular to a bimolecular recombination mechanism considering the Mott—Cohen—Fritzsche—Ovshinsky model.<sup>6</sup> However, the intermediate  $\gamma$  value between 1.0 and 0.5, which is commonly observed in *a*-Si:H photoconductivity, cannot be explained by their model. On the other hand, Rose<sup>8</sup> presented a relation  $\gamma = T_C / (T_C + T)$  for the case where conduction-band tail states are distributed exponentially and free electrons recombine with trapped holes.  $T_C$  is the characteristic temperature which represents the width of the band-tail-state profile and  $T$  is the temperature. His model, however, cannot explain the effect of the Fermi-level position on the  $\gamma$  value.

The main purpose of this paper is to clarify the following questions. Why is  $\gamma$  not 0.5 or 1.0, but an intermediate value, and what recombination process does it reflect? In order to clearly detect the Fermi-level effect, one must change the Fermi-level position without altering the localized-state profile. The doping process changes both the Fermi level and the profile simultaneously.

In this paper the Fermi-level—position effect on photo-

conductivity in *a*-Si:H was studied by metal-oxide-semiconductor field-effect transistor (MOSFET) measurements.<sup>7</sup> The photocurrent increased when the bands were bent by positive gate biases. The illumination intensity dependence of the photocurrent also changed when the Fermi level was shifted by band bending. The experimentally observed relation between the gate voltage and photocurrent was analyzed to obtain the photoconductive sensitivity as a function of the dark Fermi-level position. The obtained features are discussed considering the electron-occupation probability distribution in the band-tail states. The experimental results can be explained if the recombination rate is controlled by the capture rate of free holes by recombination centers. Finally, a comparison with doped *a*-Si:H was carried out.

### II. EXPERIMENT AND ANALYSIS

The field-effect transistor (FET) structure is illustrated by the inset in Fig. 1. The substrate was highly doped crystalline  $n^+$ -type Si and its surface was thermally oxidized to form a 0.2- $\mu\text{m}$ -thick  $\text{SiO}_2$  film. An amorphous silicon film 0.6  $\mu\text{m}$  thick was deposited by conventional rf glow discharge of silane gas, as described elsewhere.<sup>9</sup> The source and drain electrodes separated by 10  $\mu\text{m}$  were formed by aluminum evaporation onto *a*-Si:H. The gate electrode was formed by aluminum evaporation onto the opposite surface of the crystalline  $n^+$ -type Si substrate.

The gap between the source and the drain was illuminated with calibrated monochromatic light of 0.6 and 0.7  $\mu\text{m}$  wavelengths. Figure 1 shows the dark- and photo-drain current as a function of gate voltage, when a 0.2-V constant voltage was applied between the source and drain electrodes. The illumination intensity was 17  $\mu\text{W}/\text{cm}^2$ . The drain current under illumination increases monotonically when a positive gate voltage is applied. This shows that the photoconductive sensitivity increases when the bands are bent by the gate bias so that the Fermi level shifts toward the conduction-band edge. The photocurrent for a 0.7- $\mu\text{m}$ -wavelength light is more sensitive to gate voltage because the long-wavelength light, characterized by less absorption in *a*-Si:H, penetrates into the

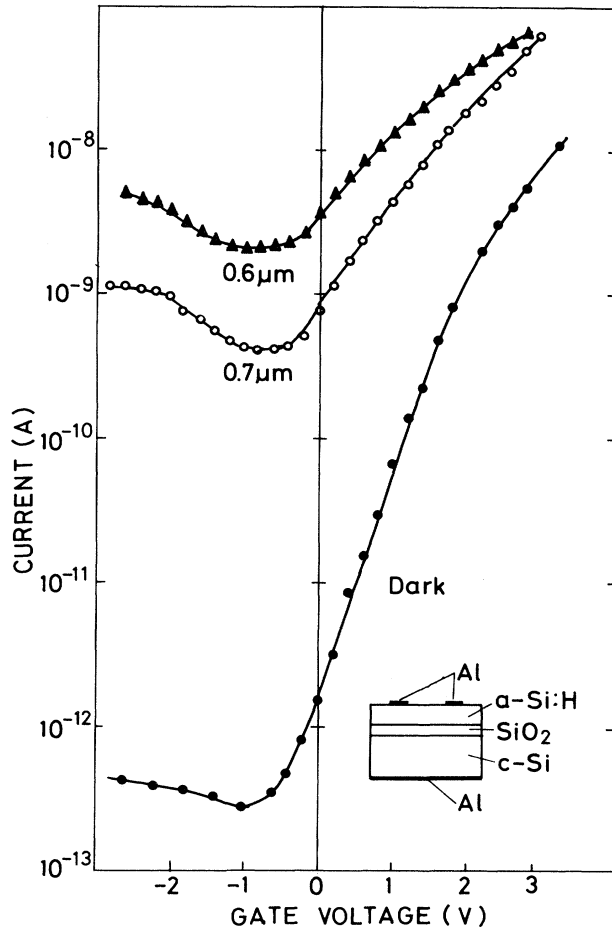


FIG. 1. Gate voltage vs drain current in the dark and under illumination. Illumination wavelengths are 0.6 and 0.7  $\mu\text{m}$  and intensity is  $17 \mu\text{W}/\text{cm}^2$ . Inset shows the structure of *a*-Si:H MOSFET samples used for the measurement.

band-bending layer. The photocurrent depends on illumination intensity  $I_0$  as  $I_0^\gamma$ . The value of  $\gamma$  varies with gate voltage, as shown in Fig. 2, which shows the relation between the illumination intensity and the photocurrent for various gate voltages. This measurement was carried out for the wavelength of 0.7  $\mu\text{m}$ . The value of  $\gamma$  is 0.86 for zero gate voltage. It continuously decreases as the positive gate bias is increased. On the other hand,  $\gamma$  is almost constant when negative gate bias is applied. The  $\gamma$  values for gate biases of  $-1.0$  and  $-2.0$  V were 0.83 and 0.82, respectively.

As photoconductive sensitivity depends on the dark Fermi-level position, the sensitivity varies with depth  $x$  in the *a*-Si:H FET. Thus the experimentally observed sensitivity  $P$  ( $\Omega\text{cm}$ ) $^{-1}$  is an integration of sensitivity over depth  $x$ . The band diagram is shown in Fig. 3. For analysis, the exponential localized-state distribution  $g(E)$ , which is usually used for the analysis of transient photocurrent,<sup>4,10</sup> is assumed to be

$$g(E) = N_1 \exp[\beta_1(E - E_0)] + N_2 \exp[(\beta_2(E_0 - E))], \quad (1)$$

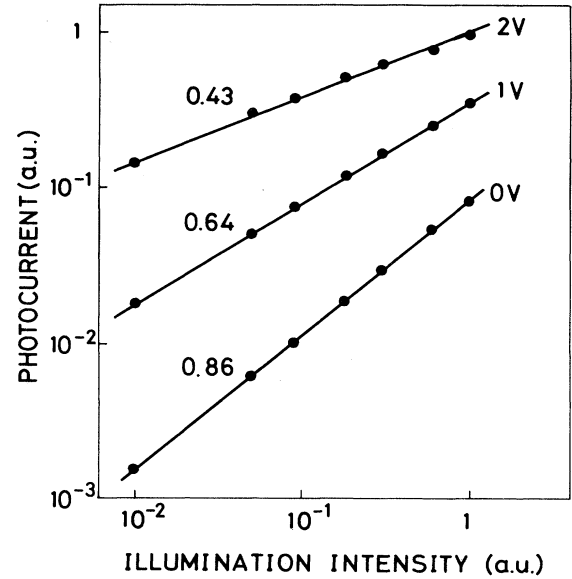


FIG. 2. Illumination intensity vs photocurrent for 0-, 1-, and 2-V gate voltages which are shown at the right-hand side of the lines. Photocurrent depends on illumination intensity  $I_0$  as  $I_0^\gamma$ .  $\gamma$  values for each gate bias are indicated by the numerals above the lines.

where  $E$  is localized-state energy. The energy  $E_0$  is set to be equal to the Fermi level at the bulk region (see Fig. 3).  $\beta_1$  and  $\beta_2$  represent distribution widths for the conduction- and valence-band tails, respectively. Poisson's equation is

$$\begin{aligned} \frac{1}{e} \frac{d^2\psi}{dx^2} &= \frac{e}{\epsilon_s} \int_{E_F - \psi}^{E_F} g(E) dE \\ &= \frac{e}{\epsilon_s} \left[ \frac{N_1}{\beta_1} (e^{\beta_1\psi} - 1) - \frac{N_2}{\beta_2} (e^{-\beta_2\psi} - 1) \right], \quad (2) \end{aligned}$$

where  $E_F$  is the Fermi energy,  $\epsilon_s$  is the permittivity of *a*-Si:H, and  $\psi$  represents the band bending. The relation  $E_F - E_0 = \psi$  was used in Eq. (2). The band bending  $\psi$  has dimensions of energy and is positive for positive gate

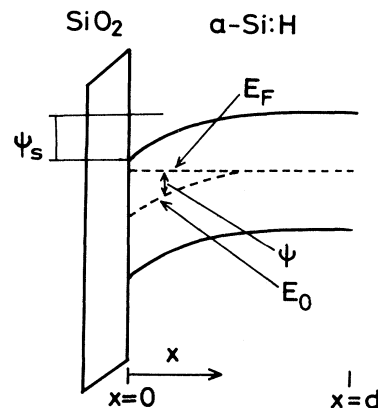


FIG. 3. Band diagram of MOSFET.

biases. The charge distribution is controlled by the trapped electrons in contrast to crystalline semiconductors,<sup>11</sup> and the electron distribution in the localized states at zero temperature is used in Eq. (2). The zero-temperature approximation is sufficiently good because the gradient of the electron distribution near the Fermi level for room temperature is much larger than that of the localized-state profile. Poisson's equation is solved to obtain the band-bending profile

$$\left[ \frac{d\psi}{dx} \right]^2 = 2 \frac{e^2}{\epsilon_s} \left[ \frac{N_1}{\beta_1} \left[ \frac{1}{\beta_1} (e^{\beta_1 \psi} - 1) - \psi \right] + \frac{N_2}{\beta_2} \left[ \frac{1}{\beta_2} (e^{-\beta_2 \psi} - 1) + \psi \right] \right] \equiv F(\psi). \quad (3)$$

Procedures similar to Ref. 11 were used to obtain Eq. (3). With the assumption that interdiffusion of carriers along a depth  $x$  within the lifetime can be neglected, the experimentally observed photoconductive sensitivity  $P$  is represented as

$$P = \frac{1}{d} \int_0^d (I_0 \alpha)^\gamma e^{-\gamma \alpha (d-x)} a(\psi) dx, \quad (4)$$

where  $\alpha$  is the absorption coefficient and  $d$  is the thickness of  $a$ -Si:H. The validity of the assumption that interdiffusion can be neglected will be discussed later.  $I_0 \alpha e^{-\alpha(d-x)}$  is the photon fraction absorbed at  $x$ , which is defined as  $x=0$  at the  $a$ -Si:H and SiO<sub>2</sub> interface and as  $x=d$  at the opposite surface of  $a$ -Si:H. It should be noted that the photoconductive sensitivity independent of the illumination intensity cannot be defined because  $\gamma$  is not unity. The conductivity at  $x$  is given by  $(I_0 \alpha e^{-\alpha(d-x)})^\gamma a(\psi)$ . A function  $a(\psi)$  related to the sensitivity at the place where the band is bent by  $\psi$  is introduced in order to clarify the mathematical procedures. Only  $(I_0 \alpha)^\gamma a(\psi)$  has a physical meaning and is the photoconductive sensitivity. It has a dimension of  $(\Omega \text{ cm})^{-1}$ . Equation (4) is expressed as the integration over  $\psi$  and then differentiated with respect to  $\psi_s$ , which is  $\psi$  at  $x=0$ , to get the sensitivity as a function of  $\psi_s$ ,

$$(I_0 \alpha)^\gamma a(\psi_s) = e^{\gamma_s \alpha d} \left[ (I_0 \alpha)^\gamma a(\psi_d) \pm d \sqrt{F(\psi_s)} \frac{dP}{d\psi_s} - \alpha d \gamma_s P \right], \quad (5)$$

where  $\psi_d = \psi(d)$ ,  $\gamma_s = \gamma(\psi_s)$ , and  $\gamma_d = \gamma(\psi_d)$ . A detailed derivation of Eq. (5) is presented in the Appendix. To obtain Eq. (5), Eq. (3) is used, assuming that  $\psi(x)$  is invariant by illumination. This assumption is valid if the number of photoexcited free electrons is sufficiently small compared with the trapped electrons at the localized states, because  $\psi(x)$  is obtained by the Poisson's equation, in which the charge distribution is determined by the trapped electrons [right-hand side of Eq. (2)]. Therefore, it is necessary to carry out the experiment using sufficient-

ly weak illumination. The validity of this assumption for this measurement will also be discussed later.

Photoconductive sensitivity is obtained as a function of the Fermi-level position using Eq. (5) and an experimental photocurrent for the 0.7  $\mu\text{m}$  wavelength. The sensitivity is  $(I_0 \alpha)^\gamma a(\psi)$ , where  $I_0 = 17 \mu\text{W}/\text{cm}^2$  and  $\alpha = 1.2 \times 10^3 \text{ cm}^{-1}$ . The absorption coefficient is determined from the transparency of  $a$ -Si:H films, which were deposited onto SiO<sub>2</sub> substrates simultaneously with FET sample films.  $N_1$  is set to  $10^{16} \text{ cm}^{-3} \text{ eV}^{-1}$  using data from capacitance-frequency technique,<sup>12</sup> and  $1/\beta_1$  is 0.1 eV, which was obtained by measuring the space-charge-limited current (SCLC) versus voltage.<sup>13</sup> The gradient  $\beta_1$  of the exponential localized-state profile obtained by the SCLC method is available for the energy region near the Fermi level. Because the level density must be continuous at the band edge, the state profile should be steeper in the energy region just below the band edge. On the other hand, experimental results on the dispersive transient photocurrent indicate that localized-state distribution is exponential over a wide energy range above the midgap.<sup>3,4</sup> Thus we assume that the exponential localized-state profile with  $1/\beta_1 = 0.1$  eV is appropriate for this analysis, because the level densities at the midgap region, where the Fermi level lies, affect the results of the analysis. The assumed localized-state profile is shown in Fig. 4. The level density at just below the conduction band, which is represented by a dotted line in Fig. 4, does not affect the analysis.

The results of the analysis are shown by the solid line in Fig. 5. The Fermi-level position is represented as  $E_C - E_F$ , where  $E_C$  is the conduction-band mobility edge. The photoconductivity is  $(I_0 \alpha)^\gamma a(\psi)$  [right-hand side of Eq. (5)], where  $\psi = E_F - E_0$ .  $E_0$  is the Fermi level at the flat-band voltage ( $E_C - E_0 = 0.7$  eV). The value of

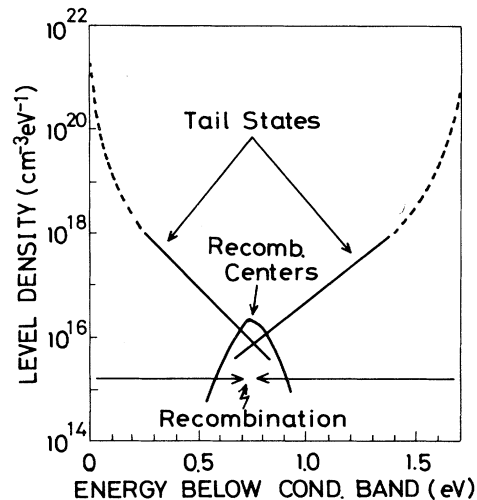


FIG. 4. Assumed localized-state profile and recombination mechanism. Level density at 0.7 eV below the conduction band is  $10^{16} \text{ cm}^{-3} \text{ eV}^{-1}$  and the gradient of the conduction-band tail is 0.1 eV which was measured by SCLC. Gradient of the valence-band tail is 0.14 eV. Nonradiative recombination takes place through the recombination centers caused by defects. Recombination centers are located at 0.6 (Ref. 18) to 0.8 eV (Ref. 20) below the conduction band.

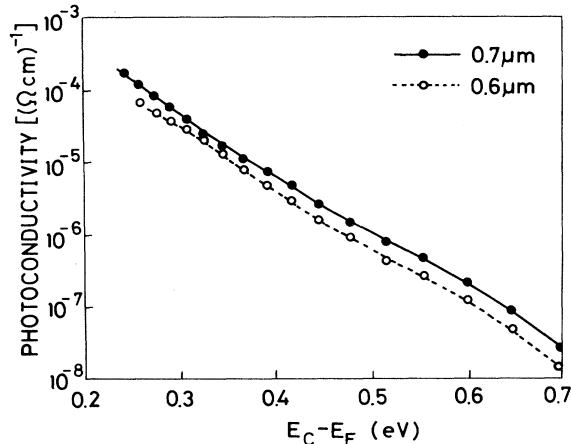


FIG. 5. Fermi-level position vs photoconductivity. Fermi-level position is indicated by the energy below the conduction-band edge. Experimental data were analyzed using Eq. (5) for  $I_0\alpha=20$  mW/cm<sup>3</sup>. Solid and dashed lines indicate analysis results for 0.7 and 0.6  $\mu$ m wavelengths, respectively. Results for the 0.6- $\mu$ m wavelength are renormalized to  $I_0\alpha=20$  mW/cm<sup>3</sup>, in accordance with the  $\alpha$  dependence of the photoconductivity in Eq. (5).

$E_C - E_0$  was determined by activation energy of the dark conductivity because temperature dependence of the Fermi level is very small for nondoped *a*-Si:H.<sup>14</sup> The obtained sensitivity depends greatly on the assumed flat-band voltage. The flat-band voltage was determined so that the sensitivity at  $E_C - E_F = 0.7$  eV was equal to the bulk photoconductive sensitivity measured using *a*-Si:H deposited on a SiO<sub>2</sub> substrate with the same condition as for FET samples. The bulk photoconductivity is  $2.6 \times 10^{-8}$  (Ω cm)<sup>-1</sup> for an intensity of  $17 \mu$ W/cm<sup>2</sup> and a wavelength of 0.7  $\mu$ m. The flat-band voltage is  $-0.1$  V.  $(I_0\alpha)^{\gamma_d} a(\psi_d)$  was determined from the photoconductive sensitivity at zero gate bias. The sensitivity is exponentially dependent on the Fermi-level position. It should be noted that this dependence changes with illumination intensity because the photocurrent does not linearly depend on the illumination intensity. Figure 5 shows the dependence for  $I_0\alpha=20$  mW/cm<sup>3</sup>. However, the principal feature, that photocurrent increases monotonically when the Fermi level becomes close to the conduction band, is not changed by the illumination intensity.

The validities of the two assumptions made in the analysis of experimental data are now discussed. First, the interdiffusion of carriers along a depth  $x$  within the carrier lifetime was ignored. If this interdiffusion is significant, the experimentally observed photoconductivity cannot be expressed by the integration of sensitivity distribution along  $x$  as was done in Eq. (4). As the photoexcitation intensity distribution along  $x$  depends on the absorption coefficient  $\alpha$ , the results of analysis for two different wavelengths, 0.6 and 0.7  $\mu$ m, were compared. The sensitivities obtained by analysis using Eq. (5) for these two wavelengths will disagree if the interdiffusion is significant. The absorption coefficient is  $2.9 \times 10^4$  cm<sup>-1</sup> for a

wavelength of 0.6  $\mu$ m. Photoconductive sensitivities, obtained from experimental data for the 0.6- $\mu$ m wavelength and renormalized following the  $\alpha$  dependence of sensitivity in Eq. (5), are represented by the dashed-line curve in Fig. 5. The good agreement between results obtained from different wavelengths indicates that Eq. (4) holds true. Second, the band bending  $\psi(x)$  was assumed to be unchanged when weak illumination is applied. In the present measurement the illumination intensity is  $17 \mu$ W/cm<sup>2</sup> and the photoconductivity is  $6 \times 10^{-6}$  (Ω cm)<sup>-1</sup> at  $E_C - E_F = 0.4$  eV, as shown in Fig. 5, for example. This corresponds to a  $3.7 \times 10^{13}$ -cm<sup>-3</sup> photoexcited electron density, assuming that electron mobility is  $1$  cm<sup>2</sup>/V s. On the other hand, electron density at the localized states which determine band bending on the right-hand side of Eq. (2) is estimated to be  $1.9 \times 10^{16}$  cm<sup>-3</sup>, using parameters already mentioned. It appears that the Poisson's equation is not affected by the photocreated free electrons and that the band bending  $\psi(x)$  is invariant for weak illumination in this experiment.

### III. DISCUSSION

#### A. Sensitivity and illumination power dependence

The reduction in the  $\gamma$  value has previously been explained by the transition from the monomolecular to the bimolecular recombination mechanism.<sup>6</sup> In this model  $\gamma$  should change suddenly from 1.0 to 0.5 when the recombination mechanism changes and the phenomenon in which  $\gamma$  varies gradually and takes an intermediate value between 0.9 and 0.3 cannot be explained. Furthermore, the dependence of the sensitivity on the Fermi-level position must change as a result of the transition in the recombination mechanism in contradiction with experimental results. In this section we calculate photoconductivity as a function of illumination intensity taking into account the distribution of photoexcited electrons and holes in localized and extended states. Figure 4 schematically illustrates the distribution of localized states and the recombination mechanism. Two kinds of localized states, which are exponentially profiled band-tail states and recombination centers caused by defects, are considered. In the calculation of photoexcited carrier distribution it is sufficient to consider only the tail states because the level density per unit volume is much larger than that of recombination centers. The distribution of carriers in the localized states is calculated from detailed balance assuming a weak electron-phonon coupling for the multiphonon trapping process by the localized states. The recombination centers play a dominant role in the nonradiative recombination, and recombination is thought to be rate limited by the hole-capture process of trapped electrons at the recombination centers. The recombination through other localized states is ignored.

The number of free electrons captured by the localized states at energy  $E$  per unit time is given by

$$N_C g(E) \nu_e(E) \{ f_C [1 - f(E)] - e_c f(E) (1 - f_C) \}, \quad (6)$$

$$e_c \equiv \exp[-(E_C - E)/kT],$$

where  $N_C$  and  $g(E)$  are level densities of the conduction

band and localized states at energy  $E$ . The first and second terms in (6) represent the number of trapped and detrapped electrons, respectively. The notations  $f_C$  and  $f(E)$  represent the occupation probability of the conduction band and localized states at energy  $E$ , and  $v_e(E)$  and  $e_c v_e(E)$  are the trapping and detrapping rate of electrons. Similarly, the number of free holes captured by the states at energy  $E$  per unit time is given by

$$N_V g(E) v_h(E) \{f(E)(1-f_v) - e_v f_v [1-f(E)]\}, \quad (7)$$

$$e_v \equiv \exp[-(E-E_V)/kT],$$

where  $N_V$  is the valence-band level density and  $f_v$  is the occupation probability of electrons at the valence band. The value of  $v_h(E)$  and  $e_v v_h(E)$  are the trapping and detrapping rates of holes. At steady state the number of captured electrons and holes by a localized state per unit time must be equal to each other because the electron occupation probability is constant with time. Thus  $f(E)$  can be represented as

$$f(E) = \frac{N_C v_e f_c + N_V e_v v_h f_v}{N_C v_e [e_c(1-f_C) + f_C] + N_V v_h (1-f_v + e_v f_v)} \quad (8)$$

by equating (6) and (7). The capture rate of trapped electrons by other localized states is neglected. The densities of free carriers are the sums of the thermal equilibrium density and photoexcited excess carrier density

$$N_C f_C = n + N_C \exp[-(E_C - E_F)/kT], \quad (9)$$

$$N_V (1-f_v) = p + N_V \exp[-(E_F - E_V)/kT], \quad (10)$$

where  $n$  and  $p$  are the densities of excess free electrons and holes and  $E_V$  is the valence-band energy.  $E_C - E_F$  and  $E_F - E_V$  are assumed to be much greater than  $kT$ . Occupation probability  $f(E)$  is obtained as

$$f(E) = \frac{An - Bp + 1}{nA(1-e_c) + pB(1-e_v) + 1 + e_f}, \quad (11)$$

$$e_f \equiv \exp[(E_F - E)/kT],$$

$$A \equiv \left[ \frac{N_V}{N_C} \frac{v_h(E)}{v_e(E)} e_v + \exp\left[-\frac{E_C - E_F}{kT}\right] \right]^{-1},$$

$$B \equiv \left[ \frac{N_C}{N_V} \frac{v_e(E)}{v_h(E)} \exp\left[-\frac{E_C - E_F}{kT}\right] + e_v \right]^{-1}$$

$$= \frac{N_V}{N_C} \frac{v_h(E)}{v_e(E)} A.$$

The approximations  $1 - \exp[-(E_C - E_F)/kT] \approx 1$  and  $1 - \exp[-(E_F - E_V)/kT] \approx 1$  are used to obtain Eq. (11). It should be noted that  $f(E)$  of Eq. (11) is equal to the Fermi-Dirac distribution in the dark ( $n=p=0$ ). The charge neutrality condition is

$$n - p + \int_{E_V}^{E_C} g(E) [f(E) - f_0(E)] dE = 0, \quad (12)$$

where  $f_0$  represents the Fermi-Dirac distribution.

The trapping process of free carriers is considered to be a multiphonon process, and it is reported that electron-

phonon coupling in  $a$ -Si:H is weak for the multiphonon trapping process by the localized states.<sup>15</sup> For weak coupling, trapping rates are

$$v_e(E) = v_{e0} \exp[-\theta_1(E_C - E)/\hbar\omega], \quad (13)$$

$$v_h(E) = v_{h0} \exp[-\theta_2(E - E_V)/\hbar\omega], \quad (14)$$

where  $\hbar\omega$  is the phonon energy and  $\theta_1$  and  $\theta_2$  are constants.<sup>16</sup> The optical phonon energy 0.06 eV of crystalline Si is used for  $\hbar\omega$ . As the hole- (electron-) capture rate is very small for the localized states near the conduction (valence) band, a detailed balance is achieved by balancing the trapping and detrapping of electrons (holes).

Equation (12) was solved numerically for each excess electron density  $n$  to obtain excess hole density  $p$  and electron-occupation probability  $f(E)$  in the localized states. The calculated occupation probabilities of electrons and holes,  $f(E)$  and  $1-f(E)$ , are shown in Fig. 6. The parameters used are  $N_V/N_C = 1.0$ ,  $v_{h0}/v_{e0} = 5 \times 10^2$ ,  $\theta_1 = \theta_2 = 1.1$ ,  $1/\beta_2 = 0.14$  eV, and  $E_C - E_V = 1.7$  eV. The value of  $v_{h0}/v_{e0}$  is consistent with the analysis of the temperature dependence of the drift mobility obtained from the time-of-flight experiment using weak electron-phonon coupling for the trapping process by localized states.<sup>17</sup> Other parameters were determined so that the calculated

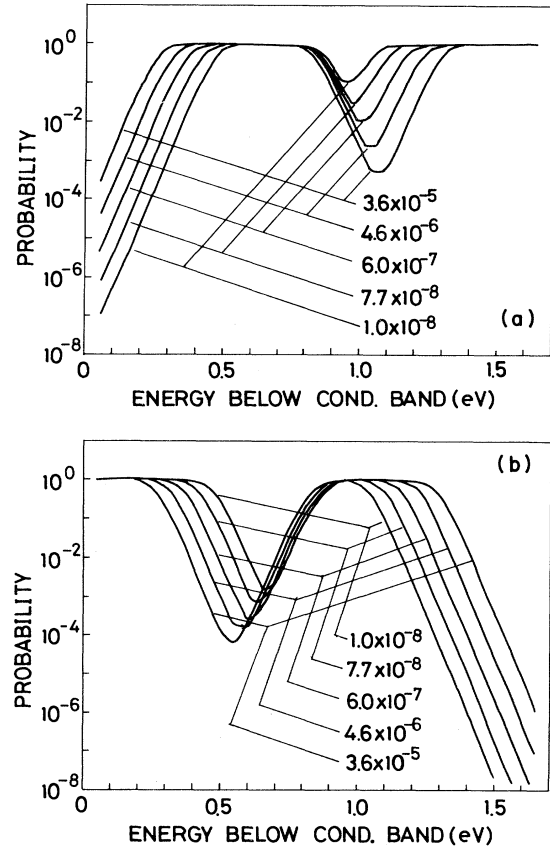


FIG. 6. Calculated occupation probability distributions of (a) electrons and (b) holes for  $E_C - E_F = 0.7$  eV. Excess electron density  $n$  per conduction-band-level density  $N_C$  is represented in the figure.

$\gamma$  value agrees with the experimentally obtained  $\gamma$ . The obtained probability distributions are very reasonable. The electron-occupation probability distribution at just below the conduction band can be expressed as  $\exp[-(E - E_{Fe})/kT]$ , and that for holes at just above the valence band is  $\exp[-(E_{Fh} - E)/kT]$ , where  $E_{Fe}$  and  $E_{Fh}$  are the quasi-Fermi levels for electrons and holes, respectively. For intense illumination intensity,  $E_{Fe}$  and  $E_{Fh}$  move toward  $E_C$  and  $E_V$ , respectively. The electron-(hole-) occupation probability at the quasi-Fermi level of holes (electrons) is reduced by illumination because the summation of electron- and hole-occupation probability must be 1.0. These fundamental features are invariant with respect to the parameters used. It should be further noted that the localized-state densities at just below the conduction band and just above the valence band, represented by dotted lines in Fig. 4, do not affect the calculated results because  $f(E) - f_0(E)$  is extremely small for these states.

It has been reported that the recombination centers  $D_2$  caused by the dangling bonds dominate the nonradiative-recombination process.<sup>18</sup> For recombination through the recombination centers, two important processes are free-electron capture by holes at the centers and free-hole capture by electrons at the centers. In the steady state the capture rates of electrons and holes are equal to each other,

$$v_e \sigma_e n (1 - f_R) = v_h \sigma_h p f_R, \quad (15)$$

where  $f_R$ ,  $v_e$ , and  $v_h$  are the electron-occupation probability at the recombination centers, thermal velocity of free electrons, and thermal velocity of free holes, respectively. The capture cross sections of electrons and holes are represented by  $\sigma_e$  and  $\sigma_h$ . The detrapping probability from the recombination centers is ignored. In the steady state excitation and recombination are balanced. Thus

$$dn/dt = I_0 \alpha - N_R v_e \sigma_e n (1 - f_R) = 0, \quad (16)$$

and we obtain

$$I_0 \alpha = \frac{N_R \sigma_e n v_e \sigma_h p v_h}{\sigma_e n v_e + \sigma_h p v_h}, \quad (17)$$

where  $N_R$  is the recombination-center density and  $I_0 \alpha$  is the photoexcitation rate. The recombination rate [Eq. (17)] is limited by the electron- or hole-capture rate, whichever is smaller than the other type of carrier capture rate. For  $\sigma_h p v_h \gg \sigma_e n v_e$ ,  $I_0 \alpha$  is proportional to  $n$  and  $\gamma = 1$  in contradiction with the experimental results. This corresponds to the monomolecular recombination. Thus  $\sigma_e n v_e$  must be larger than or comparable with  $\sigma_h p v_h$ .

The capture cross sections depend on the type of recombination centers. If the recombination centers are donorlike (acceptorlike), the ratio  $\sigma_e/\sigma_h$  is about  $10^3$  ( $10^{-3}$ ) which is a typical ratio for capture cross sections of charged and neutral centers.<sup>19</sup> The relation between  $n$  and  $p$  was calculated by solving Eq. (12) numerically. Then photoconductivity was obtained as functions of illumination intensity from Eq. (17) for these two cases. First, we discuss the case where the recombination centers are donorlike. The case where the centers are acceptorlike is

discussed at the end of this section.

The calculated results are presented in Fig. 7. To obtain the illumination intensity  $I_0 \alpha$  and the photoconductivity  $en\mu_0$  from the values of  $p$  and  $n$ , the following constants were used: i.e.,  $N_R = 10^{16} \text{ cm}^{-3}$ ,  $\sigma_h = 5 \times 10^{-16} \text{ cm}^2$ ,  $v_h = 10^7 \text{ cm/s}$ ,  $N_C = 10^{20} \text{ cm}^{-3}$ , and electron mobility  $\mu_0 = 1 \text{ cm}^2/\text{Vs}$ . A typical cross section of  $5 \times 10^{-16} \text{ cm}^2$  for neutral centers was used for  $\sigma_h$  because donorlike centers are neutral when they are not occupied by electrons. The value of  $\sigma_e$  does not affect the results because  $\sigma_e n \gg \sigma_h p$  and  $I_0 \alpha = N_R \sigma_h v_h p$  for the case where  $\sigma_e > \sigma_h$ . Therefore, the recombination rate is limited by the hole-capture process of the recombination centers. A typical spin density for nondoped *a*-Si:H was used for  $N_R$ . The observed photocurrent was thought to be carried by electrons at the conduction band. The calculated photoconductivity in Fig. 6 increases monotonically with the reduction in  $E_C - E_F$  and is consistent with the experimental results. The ratio of photoexcited electron density  $n$  at the conduction band to the total photoexcited electron density depends on the Fermi-level position in the dark. For a large  $E_C - E_F$ , almost all the excited electrons are trapped by the localized states. The ratio increases when  $E_C - E_F$  is reduced because the localized states below the Fermi level are already occupied at dark and cannot trap the photoexcited electrons. Thus the fraction of excited electrons which contribute to the photoconductivity increases. This is the reason why the photoconductive sensitivity increases when the Fermi level shifts toward the conduction band.

The  $\gamma$  value is plotted as a function of the Fermi-level position in Fig. 8. The solid circles and the solid line

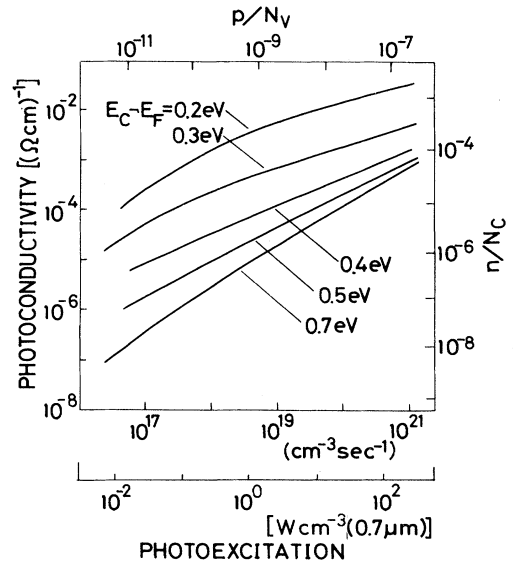


FIG. 7. Calculated relation between photoexcitation intensity and photoconductivity for  $E_C - E_F = 0.2 - 0.7 \text{ eV}$ . Photoexcitation intensity is represented by two units, i.e., absorbed photon density and energy at the wavelength of  $0.7 \mu\text{m}$ . Corresponding excess electron and hole densities are shown on the right-hand and upper sides, respectively.

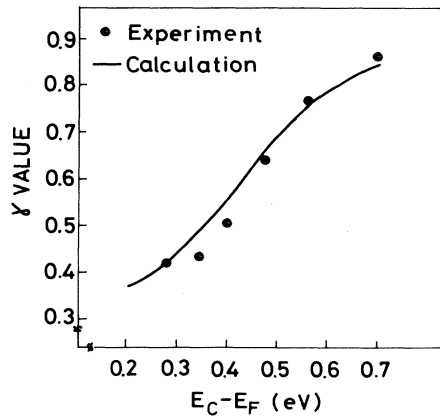


FIG. 8. Fermi-level—position dependence of the exponent  $\gamma$ . Closed circles and solid line represent the experimental and calculated results, respectively.

represent experimental and theoretical results, respectively. The experimental  $\gamma$  value was obtained by the following procedure. Differentiating  $\ln P$  [ $P$  is expressed by Eq. (4)] with respect of  $\ln I_0 \alpha$ , we obtain

$$\frac{d \ln P}{d \ln(I_0 \alpha)} = \frac{1}{P} \frac{1}{d} \int_0^d \gamma(I_0 \alpha)^\gamma e^{-\gamma \alpha(d-x)} a(\psi) dx$$

$$= \gamma_{\text{eff}} \approx \gamma_s \quad (18)$$

The definition of  $\gamma_{\text{eff}}$  and the relation  $\gamma_{\text{eff}} \approx \gamma_s$  are discussed in the Appendix. Thus the  $\gamma$  value at the Fermi-level position  $E_F$  is equal to the experimentally observed  $\gamma$  at gate voltage  $V_G$  at which  $\psi_s(V_G) = E_F - E_0$ . On the other hand, the calculated  $\gamma$  value was obtained from the gradient of the  $\ln I_0 \alpha - \ln n$  plot in Fig. 6. When  $E_C - E_F$  is as small as 0.3 eV, the calculated photocurrent does not simply depend on photoexcitation intensity as  $(I_0 \alpha)^\gamma$  but the gradient of the  $\ln I_0 \alpha - \ln n$  plot increases for weak illumination. In this case, the  $\gamma$  value was obtained by least-squares fitting in the region of  $I_0 \alpha = 10^{-1} - 10^2$  W/cm<sup>3</sup>. The agreement between experimental and calculated results is good. It should be noted that the  $\gamma$  variation between 0.35 and 0.85 can be explained by the model without assuming any transition in the recombination mechanism. According to Rose's relation  $\gamma = T_C / (T_C + T)$ ,  $\gamma$  is 0.8 for  $T_C = 1200$  K. A much larger  $T_C$  must be assumed to explain the observed  $\gamma$  which is larger than 0.8. On the other hand, a  $\gamma$  smaller than 0.5 cannot be explained by the simple bimolecular recombination mechanism. However,  $\gamma$  larger than 0.8 and smaller than 0.5 can be explained by our model.

Let us consider the case where the recombination centers are acceptorlike. As  $n$  is much larger than  $p$ ,  $\sigma_h v_h p$  is not sufficiently larger than  $\sigma_e v_e n$  even if  $\sigma_h / \sigma_e$  is as large as  $10^3$ , thus  $\gamma$  is not equal to 1.0. The estimated  $\gamma$ , however, is larger than that for the case of donorlike recombination centers, and does not agree with the experimental results. Moreover, the calculated photoconductive sensitivity is much smaller than the observed one. Var-

deny *et al.* have observed deep levels with  $\sigma_h = 10^{-13}$  cm<sup>2</sup> by the experiment of picosecond photoinduced absorption, and have attributed the large cross section to the negatively charged levels.<sup>21</sup> From the results of our calculation, we find that the reported negatively charged levels have no significant effects on the recombination at room temperature.

#### B. Comparison with doped samples

Anderson *et al.* investigated doped *a*-Si:H photoconductivity. Although sensitivity increases as a result of light phosphorus doping, it saturates and then decreases when phosphorus is heavily doped to make  $E_C - E_F$  smaller than 0.4 eV.<sup>6</sup> On the other hand, sensitivity increases monotonically when the Fermi level shifts toward the conduction-band edge due to field effect in this measurement. These results indicate that impurity doping causes defects which reduce the photoconductive sensitivity and that purely Fermi-level—position effects on photoconductivity cannot be detected by impurity doping. Thus the sensitivity saturation at  $E_C - E_F = 0.4$  eV for phosphorus-doped samples is not due to the Fermi-level shift.

Anderson *et al.* also have reported that the illumination-intensity dependence factor  $\gamma$  for photocurrent varies when the Fermi level shifts toward the conduction band due to phosphorus doping.<sup>6</sup> They attributed this phenomena to a change in the recombination mechanisms because the sensitivity saturates at the doping level where  $\gamma$  changes. They further stated that a peak in the localized-state density at 0.4 eV below  $E_C$  causes the change in the recombination mechanism. Similar photoconductive data were reported by Vanier *et al.*<sup>22</sup> The latter attributed the maximum sensitivity at  $E_C - E_F = 0.4$  eV to the minimum point in the localized-state density which lies 0.4 eV below  $E_C$ . This is contrary to the report by Anderson *et al.* However, it is clear that the saturation and decrease in sensitivity are due to defects caused by impurity doping, as already discussed. Sensitivity increases monotonically when  $E_C - E_F$  is reduced by the field effect. Furthermore,  $\gamma$  varies gradually rather than abruptly as a result of the Fermi-level shift, as shown in Fig. 7. It is thought that the change in the recombination mechanism does not occur as a result of the Fermi-level shift caused by the field effect.  $\gamma$  varies with the Fermi-level position, even if the recombination mechanism does not change as already discussed.

According to the SCLC measurement,  $T_C$  varies between 1200 and 300 K as a result of phosphorus doping.<sup>23</sup> As the  $\gamma$  value is strongly affected by  $T_C$ , the variation in phosphorus-doped *a*-Si:H, which was reported by Anderson *et al.*, is not due to the Fermi-level shift but due to the change in the conduction-band-tail profile.

#### IV. SUMMARY

The Fermi-level—position effect on photoconductivity in *a*-Si:H was investigated using MOSFET's. The Fermi level was shifted using the field effect without causing any changes in the localized-state profile. The sensitivity in-

creases exponentially when the Fermi level becomes close to the conduction band and does not saturate in contrast to doped *a*-Si:H. The illumination-power dependence factor  $\gamma$  of photocurrent varies with the Fermi-level position.

These features can be explained without making the assumption that the recombination mechanism changes as the Fermi level shifts. The recombination rate is proportional to the product of free-hole density and trapped-electron density at recombination centers, i.e., it is limited by the capture process of free holes by trapped electrons at recombination centers. The illumination-intensity dependence factor  $\gamma$  depends on the conduction-band-tail-state profile and the Fermi-level position.

#### ACKNOWLEDGMENTS

The authors would like to express their thanks to Dr. N. Kuroyanagi and Dr. S. Hashimoto for encouragement throughout this work. They would also like to express thanks to Dr. S. Furukawa for his helpful discussions.

#### APPENDIX

The derivation of Eq. (5) is presented in this Appendix. Integration over  $x$  in Eq. (4) is transferred to integration over  $\psi$

$$P = \frac{1}{d} \int_{\psi_s}^{\psi_d} (I_0 \alpha)^\gamma e^{-\gamma \alpha (d-x)} a(\psi) \frac{\partial x}{\partial \psi} d\psi, \quad (\text{A1})$$

where  $\gamma$  depends on  $\psi$  and  $x$  depends on  $\psi$  and  $\psi_s$  as

$$x = \mp \int_{\psi_s}^{\psi} \frac{d\psi}{\sqrt{F(\psi)}}. \quad (\text{A2})$$

A general formula,

$$\begin{aligned} \frac{d}{d\psi_s} \int_{\psi_s}^{\psi_d} \Phi(\psi_s, \psi) d\psi &= \Phi(\psi_s, \psi_d) \frac{d\psi_d}{d\psi_s} - \Phi(\psi_s, \psi_s) \\ &+ \int_{\psi_s}^{\psi_d} \frac{\partial \Phi}{\partial \psi_s} d\psi, \end{aligned} \quad (\text{A3})$$

can be used to differentiate (A1) with respect to  $\psi_s$ . Set-

ting

$$\Phi(\psi_s, \psi) = (I_0 \alpha)^\gamma e^{-\gamma \alpha (d-x)} a(\psi) \frac{\partial x}{\partial \psi}, \quad (\text{A4})$$

we obtain

$$\begin{aligned} \frac{dP}{d\psi_s} &= \mp \frac{1}{d} (I_0 \alpha)^{\gamma_d} a(\psi_d) \frac{1}{\sqrt{F(\psi_d)}} \frac{d\psi_d}{d\psi_s} \\ &\pm \frac{1}{d} (I_0 \alpha)^{\gamma_s} e^{-\gamma_s \alpha d} a(\psi_s) \frac{1}{\sqrt{F(\psi_s)}} \\ &+ \frac{1}{d} \int_{\psi_s}^{\psi_d} (I_0 \alpha)^\gamma \alpha \gamma \frac{\partial x}{\partial \psi_s} e^{-\gamma \alpha (d-x)} a(\psi) \frac{\partial x}{\partial \psi} d\psi, \end{aligned} \quad (\text{A5})$$

where  $\partial x / \partial \psi = \mp 1 / \sqrt{F(\psi)}$  was used. The last term in Eq. (A5) can be written as  $\pm \gamma_{\text{eff}} \alpha P / \sqrt{F(\psi_s)}$  because  $\partial x / \partial \psi_s = \pm 1 / \sqrt{F(\psi_s)}$  is independent of  $\psi$ , and  $\gamma$  has a weak dependence on  $\psi$  compared with other factors. The value of  $\gamma_{\text{eff}}$  is almost equal to  $\gamma_s$  because  $a(\psi)$  is maximum at  $\psi = \psi_s$ . Since

$$d = \mp \int_{\psi_s}^{\psi_d} \frac{d\psi}{\sqrt{F(\psi)}} \quad (\text{A6})$$

is constant,

$$\frac{d\psi_d}{d\psi_s} = \left[ \frac{F(\psi_d)}{F(\psi_s)} \right]^{1/2}. \quad (\text{A7})$$

So (A5) can be written as

$$\begin{aligned} \frac{dP}{d\psi_s} &= \mp \frac{1}{\sqrt{F(\psi_s)}} \left[ \frac{1}{d} (I_0 \alpha)^{\gamma_d} a(\psi_d) \right. \\ &\left. - \frac{1}{d} (I_0 \alpha)^{\gamma_s} e^{-\gamma_s \alpha d} a(\psi_s) - \gamma_s \alpha P \right]. \end{aligned} \quad (\text{A8})$$

Equation (5) can be obtained directly from (A8).

<sup>1</sup>R. A. Street, Phys. Rev. B **21**, 5775 (1980).

<sup>2</sup>P. W. Collins and W. Paul, Phys. Rev. B **25**, 5762 (1982).

<sup>3</sup>J. M. Hvam and M. H. Brodsky, Phys. Rev. Lett. **46**, 371 (1981).

<sup>4</sup>T. Kagawa, S. Furukawa, and N. Matsumoto, Phys. Rev. B **26**, 4714 (1982).

<sup>5</sup>Z. Vardeny, P. O'Connor, S. Ray, and J. Tauc, Phys. Rev. Lett. **44**, 1267 (1980).

<sup>6</sup>D. A. Anderson and W. E. Spear, Philos. Mag. **36**, 695 (1977).

<sup>7</sup>N. Matsumoto, T. Kagawa, and S. Furukawa, in Proceedings of the 16th International Conference on the Physics of Semiconductors, Montpellier, 1982, edited by M. Averous [Physica **117-118B-C**, 929 (1983)]; W. B. Jackson and M. J. Thompson, *ibid.*, p. 883.

<sup>8</sup>A. Rose, RCA Rev. **12**, 362 (1951).

<sup>9</sup>T. Kagawa, N. Matsumoto, and K. Kumabe, Jpn. J. Appl. Phys. **21**, Suppl. 21-1, 251 (1982).

<sup>10</sup>T. Tiedje, J. M. Cebulca, D. M. Morel, and B. Abeles, Phys. Rev. Lett. **46**, 1425 (1981).

<sup>11</sup>S. M. Sze, *Physics of Semiconductor Devices* (Wiley, New York, 1969), p. 431.

<sup>12</sup>P. Viktorovich and G. Moddel, J. Appl. Phys. **51**, 4847 (1980).

<sup>13</sup>S. Furukawa, T. Kagawa, and N. Matsumoto, Solid State Commun. **44**, 927 (1982).

<sup>14</sup>D. H. Jones, P. G. LeComber, and W. E. Spear, Philos. Mag. **36**, 541 (1977).

<sup>15</sup>H. Ohkushi, T. Tokumaru, S. Yamasaki, H. Oheda, and K. Tanaka, Phys. Rev. B **25**, 4313 (1982).

<sup>16</sup>N. F. Mott, Solid-State Electron. **21**, 1275 (1978).

<sup>17</sup>T. Kagawa and N. Matsumoto, Proceedings of the 10th International Conference on Amorphous and Liquid Semiconductors, Tokyo, 1983 (unpublished).

<sup>18</sup>K. Morigaki, Y. Sano, and J. Hirabayashi, Solid State Commun. **39**, 947 (1981).

- <sup>19</sup>M. Lax, Phys. Rev. 119, 1502 (1960).
- <sup>20</sup>J. D. Cohen, J. P. Harbison, and K. W. Wecht, Phys. Rev. Lett. 48, 109 (1982).
- <sup>21</sup>Z. Vardeny, J. Strait, D. Pfof, and J. Tauc, Phys. Rev. Lett. 48, 1132 (1982).
- <sup>22</sup>P. E. Vanier, A. E. Delahoy, and R. W. Griffith, in *Tetrahedrally Bonded Amorphous Semiconductors (Carefree, Arizona)*, Topical Conference on Tetrahedrally Bonded Amorphous Semiconductors, edited by R. A. Street, D. K. Biegelsen, and J. C. Knights (AIP, New York, 1981), p. 227.
- <sup>23</sup>S. Furukawa and N. Matsumoto, Phys. Rev. B 27, 4955 (1983).